University of South Florida

Scholar Commons

USF Libraries Florida COVID Research Collection publications

USF Libraries Florida COVID-19 Research Collections

9-2020

Disentangling the Impact of the COVID-19 Lockdowns on Urban NO$_2$ from Natural Variability

Daniel L. Goldberg
George Washington University

Susan C. Anenberg
George Washington University

Debora Griffin
Air Quality Research Division, Environment and Climate Change Canada (ECCC), Toronto

Chris A McLinden
Air Quality Research Division, Environment and Climate Change Canada (ECCC), Toronto

Zifeng Lu
Energy Systems Division Argonne National Laboratory, Lemont, IL

See next page for additional authors

Follow this and additional works at: https://scholarcommons.usf.edu/usf_fcrc_all

Scholar Commons Citation

Goldberg, Daniel L.; Anenberg, Susan C.; Griffin, Debora; McLinden, Chris A; Lu, Zifeng; and Streets, David G., "Disentangling the Impact of the COVID-19 Lockdowns on Urban NO$_2$ from Natural Variability" (2020).
USF Libraries Florida COVID Research Collection publications. 15.
https://scholarcommons.usf.edu/usf_fcrc_all/15

Authors

Daniel L. Goldberg, Susan C. Anenberg, Debora Griffin, Chris A McLinden, Zifeng Lu, and David G. Streets

Key Points:
- Meteorological patterns were especially favorable for low NO_2 in much of the United States in spring 2020, complicating comparisons with spring 2019
- Weather variations between years can cause column NO_2 differences of ~15% over monthly timescales
- NO_2 drops attributed to COVID-19 lockdowns ranged between 9.2% and 43.4% among 20 cities in North America, with a median of 21.6%

Supporting Information:
- Supporting Information S1

Correspondence to:
D. L. Goldberg,
dgoldberg@gwu.edu

Author Contributions:
Conceptualization: Daniel L. Goldberg, Susan C. Anenberg, Zifeng Lu
Data curation: Debora Griffin, Chris A. McLinden, Zifeng Lu
Formal analysis: Daniel L. Goldberg, Debora Griffin, Chris A. McLinden
Writing - original draft: Daniel L. Goldberg
(continued)

Disentangling the Impact of the COVID-19 Lockdowns on Urban NO₂ From Natural Variability

Daniel L. Goldberg[1,2] , **Susan C. Anenberg**[1] , **Debora Griffin**[3] , **Chris A. McLinden**[3] , **Zifeng Lu**[2] , and **David G. Streets**[2]

[1]Department of Environmental and Occupational Health, George Washington University, Washington, DC, USA, [2]Energy Systems Division, Argonne National Laboratory, Lemont, IL, USA, [3]Air Quality Research Division, Environment and Climate Change Canada (ECCC), Toronto, Ontario, Canada

Abstract TROPOMI satellite data show substantial drops in nitrogen dioxide (NO_2) during COVID-19 physical distancing. To attribute NO_2 changes to NO_x emissions changes over short timescales, one must account for meteorology. We find that meteorological patterns were especially favorable for low NO_2 in much of the United States in spring 2020, complicating comparisons with spring 2019. Meteorological variations between years can cause column NO_2 differences of ~15% over monthly timescales. After accounting for solar angle and meteorological considerations, we calculate that NO_2 drops ranged between 9.2% and 43.4% among 20 cities in North America, with a median of 21.6%. Of the studied cities, largest NO_2 drops (>30%) were in San Jose, Los Angeles, and Toronto, and smallest drops (<12%) were in Miami, Minneapolis, and Dallas. These normalized NO_2 changes can be used to highlight locations with greater activity changes and better understand the sources contributing to adverse air quality in each city.

Plain Language Summary Nitrogen dioxide (NO_2) is an air pollutant whose prevalence in urban areas is linked to fossil fuel combustion. The NO_2 in our atmosphere is primarily a function of the magnitude of nitrogen oxide (NO_x) emissions and weather factors such as sun angle, wind speed, and temperature. In this work, we developed two novel methods to account for weather impacts on daily pollution levels during COVID-19 precautions. Once we accounted for favorable weather conditions that in some cases kept air pollution low independent of tailpipe emissions, calculated air pollutant emission reductions varied dramatically (9–43%) among 20 North American cities. Results can be used to understand factors contributing to inconsistent NO_2 changes during physical distancing, which can inform the effectiveness of COVID-19 protocols and aid future policy development. These methodologies will allow us to respond more quickly in future unintended experiments when emissions change suddenly.

1. Introduction

Nitrogen dioxide (NO_2) is unique due to its relatively short photochemical lifetime, which varies from 2–6 hr during the summer daytime (Beirle et al., 2011; de Foy et al., 2014; Laughner & Cohen, 2019; Valin et al., 2013) to 12–24 h during winter (Beirle et al., 2003; Shah et al., 2020); the main loss pathway of NO_2 is reaction with OH (Stavrakou et al., 2013). Due to the relatively short lifetime of NO_2, tropospheric NO_2 concentrations are strongly correlated with local NO_x emissions, which are often anthropogenic in origin. However, due to the effects of meteorology and solar zenith angle on the NO_2 abundance, NO_2 can vary by a factor of two simply due to seasonal changes (Pope et al., 2015; Wang et al., 2019). Therefore, satellite data are typically averaged over long timeframes (approximately seasonal/annual) to assess changes in NO_x emissions (Duncan et al., 2016; Geddes et al., 2016; Georgoulias et al., 2019; Hilboll et al., 2013, 2017; Kim et al., 2009; Krotkov et al., 2016; Lamsal et al., 2015; McLinden et al., 2016; van Der et al., 2008).

With the COVID-19 crisis, there is now broad interest in rapid assessments of NO_x emission changes on short timescales in locations that have implemented stay-at-home orders or other physical distancing measures. Using satellite data in this instance can be advantageous due to its global coverage at immediate timescales. However, current methods of averaging satellite NO_2 data over many months to minimize random daily effects of weather will not provide the temporal granularity needed to quantify short-lived NO_x emission changes.

Writing – review & editing: Susan C. Anenberg, Debora Griffin, Chris A. McLinden, Zifeng Lu, David G. Streets

Preliminary satellite-based studies indicate that NO_2 dropped substantially in China following stringent COVID-19 physical distancing actions (Liu et al., 2020; Zhang et al., 2020). Similar declines have also been seen over northern Italy (ESA, 2020b) and India (ESA, 2020a). Although lockdown measures—and adherence to them—have been looser in the United States than in China, India, and Italy, preliminary analyses show that NO_2 amounts are declining across United States cities as well (NASA, 2020). These declines have, in some cases in the media (Holcombe & O'Key, 2020; Plumer & Popovich, 2020), been attributed to the emission changes during lockdowns, without accounting for the potentially substantial influences of meteorology and seasonality. Accounting for natural NO_2 fluctuations are especially important during spring, a time when the NO_2 concentrations and lifetimes are quickly changing due to transitioning meteorology, solar zenith angle, and snow cover.

Understanding how NO_x emissions have changed in response to physical distancing measures requires new methods to account for solar zenith angle and meteorological conditions over very short time scales (days/weeks), as opposed to the traditional method of averaging over seasons and years. Here, we use three different methods to assess the NO_2 decreases associated with COVID-19 lockdowns. We combine TROPOMI NO_2 data with ERA5 reanalysis and a regional chemical transport model to determine the effects of the solar zenith angle and meteorological factors—such as wind speed and wind direction—on NO_2 column amounts. The NO_2 changes after this "normalization" are more likely to represent the NO_x emissions changes due to COVID-19.

2. Methods

2.1. TROPOMI NO_2

TROPOMI was launched by the European Space Agency (ESA) for the European Union's Copernicus Sentinel 5 Precursor (S5p) satellite mission on 13 October 2017. The satellite follows a Sun-synchronous, low-Earth (825 km) orbit with a daily equator overpass time of approximately 13:30 local solar time (van Geffen et al., 2019). TROPOMI measures total column amounts of several trace gases in the Ultraviolet-Visible-Near Infrared-Shortwave Infrared spectral regions (Veefkind et al., 2012). At nadir, pixel sizes are 3.5×7 km^2 (reduced to 3.5×5.6 km^2 on 6 August 2019) with little variation in pixel sizes across the 2,600 km swath.

Using a differential optical absorption spectroscopy (DOAS) technique on the radiance measurements in the 405–465 nm spectral window, the top-of-atmosphere spectral radiances can be converted into slant column amounts of NO_2 between the sensor and the Earth's surface (Boersma et al., 2018). In two additional steps, the slant column quantity can be converted into a tropospheric vertical column content, which is the quantity used most often to further our understanding of NO_2 in the atmosphere (Beirle et al., 2019; Dix et al., 2020; Goldberg, Lu, Streets, et al., 2019; Griffin et al., 2019; Ialongo et al., 2020; Reuter et al., 2019; Zhao et al., 2020). For this analysis, we use the operational "off-line" TROPOMI NO_2 data set, Version 1.2 preceding 26 March 2019 and Version 1.3 post-27 March 2019.

2.2. Meteorological Data Set

We use ERA5 meteorology (Copernicus Climate Change Service (C3S), 2017) for the wind speed and direction in our analysis. When filtering the data based on wind, we use the average 100-m winds during 16–21 UTC, which approximately corresponds to the TROPOMI overpass time over North America. To downscale the ERA5 reanalysis, which is provided at $0.25° \times 0.25°$, we spatially interpolate daily averaged winds to $0.01° \times 0.01°$ using bilinear interpolation. Due to our dependence on $0.25° \times 0.25°$ meteorology, any microscale features (e.g., sea breezes) will not be accounted for, but these effects should be minor for our particular analysis.

2.3. Calculation of NO_2 Changes

We calculate the NO_2 changes using three different methods and a control. In the control (Method 0), a simple difference before (1 January to 29 February 2020) and after (15 March to 30 April 2020) COVID-19 precautions is calculated; this represents the true change in NO_2 column densities over time. The 15 March to 30 April 2020 period is the timeframe of the most stringent lockdown in North America—some U.S. states began to transition out of the lockdown on 1 May 2020. In Method 1, we compare an average of 15 March

to 30 April 2020 to the same timeframe of 2019 and would therefore account for impact of changes due to solar zenith angle; this year-over-year comparison is used most often in satellite studies quantifying long-term changes in NO_x emissions. In Method 2, we develop a strategy to account for varying weather patterns without the use of a chemical transport model. In this method, we normalize each day's NO_2 observation to a day with "standard" meteorology—similar to standard temperature and pressure (STP) conditions in a laboratory setting. We do this by accounting for four different day-varying effects; these are solar zenith angle, wind speed, wind direction, and day-of-week. In all cases, we normalize city-specific conditions to those that are climatological on 15 April. Finally, in Method 3, we infer a TROPOMI NO_2 column amount assuming no COVID-19 precautions using the GEM-MACH regional chemical transport model, which is operationally run in forecast mode (Pendlebury et al., 2018), and then compare the actual TROPOMI columns to the theoretical columns. Methods 2 and 3 both account for year-varying meteorology, while Method 1 does not. A detailed description of Methods 2 and 3 can be found in the supporting information.

3. Results

3.1. Solar Zenith Angle and Meteorological Relationships

In the top row of Figure 1, we show 2019 NO_2 column densities during the high solar zenith angle "cold" season (January–March and October–December) and low solar zenith angle "warm" season (May–September) in the continental United States and southern Canada.
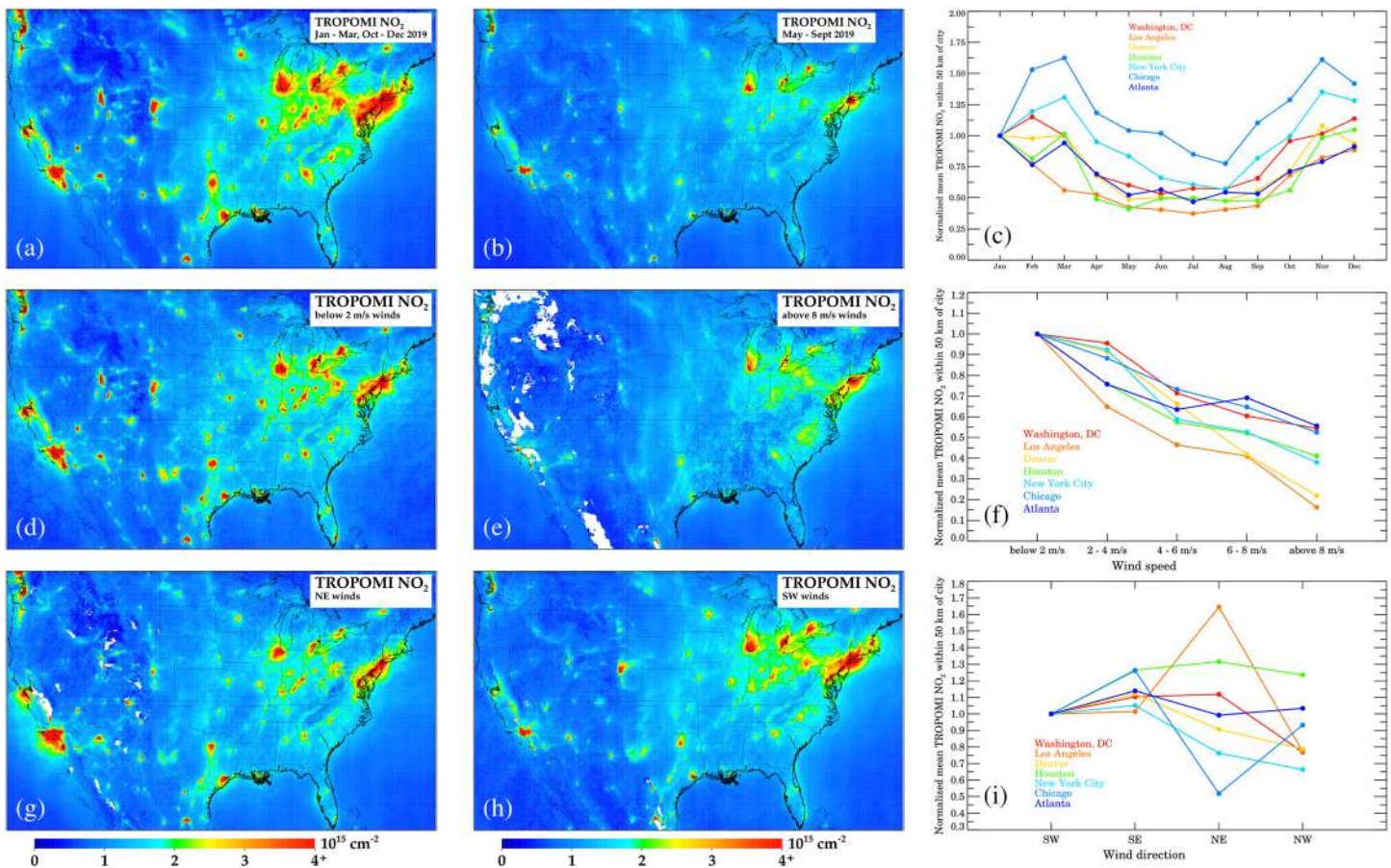
Column NO_2 is larger during the cold season than during the warm season over the majority of our domain, despite NO_x emissions generally peaking during summer months due to a heavy air conditioning load (Abel et al., 2017; He et al., 2013) and more vehicle miles traveled (https://www.transtats.bts.gov/osea/seasonaladjustment/?PageVar=VMT). The larger NO_2 concentrations during the winter are instead due to the longer NO_2 lifetime during the cold season, primarily due to slower photolysis rates. When NO_x is emitted during the warm season, it is transformed into other chemical species, such as O_3 and HNO_3, more quickly than during the winter. Also, the fraction of NO_x that is in the form of NO_2 (rather than NO) is variable, largely due to relative levels of O_3 and sunlight. We find that in most near-urban locations column NO_2 amounts are 1.5–3 times larger during the winter than during the summer and can vary substantially between city.

In a next step, we account for wind speed and wind direction in the spatiotemporal variation of NO_2 columns. In the middle and bottom panels of Figure 1, we demonstrate the effects of wind speed and wind direction on the NO_2 in our domain. Increases in wind speed yield NO_2 decreases due to quicker dispersion away from the city centers. For example, in New York City, Washington DC, Atlanta, and Chicago, all cities with relatively flat topography and located in the eastern United States, increasing wind speeds from nearly stagnant to >8 m/s decreases NO_2 by 30–60%. Conversely, in Denver and Los Angeles, cities with more heterogeneous topography and with general isolation from an agglomeration of cities show a stronger dependence on wind speed; increasing wind speeds from nearly stagnant to >8 m/s decreases NO_2 by 70–85%. In both instances, these examples show the strong dependence of wind speed on local NO_2 amounts.

Similarly, wind direction has a large role in the local NO_2 amounts, although the effects of wind direction are nonlinear. Generally, northwest winds yield the cleanest conditions in most U.S. cities, but the effects of other wind directions are more nuanced. For example, southwesterly winds yield the worst air quality in New York City, while northeasterly winds yield the largest NO_2 in Washington, D.C. This is due to the fact that the other city lies upwind in each opposing scenario. Changes in wind direction, given the same wind speed, can yield differences in NO_2 in major cities by up to 70%, and must be accounted for if properly attributing NO_2 changes to NO_x emissions. Climatological patterns for all cities are shown in the supporting information (Figures S2–S4).

While 2-m air temperature and boundary layer depth may be affecting the NO_2 concentrations, these are not independent of the aforementioned factors: solar zenith angle, wind speed, and wind direction. In fact, solar zenith angle, wind speed, and wind direction are by themselves highly skilled predictors of near-surface temperatures and boundary layer depth in most instances. Since we are focused on mostly clear-sky days, clouds have limited effects here. Previous day's precipitation may also be a contributing factor to daily NO_2 amounts, but in many areas, the wind direction will partially account for this, since northwest winds usually follow large rain events in most areas.

Figure 1. Effects of meteorology and solar zenith angle on column NO$_2$. Top panels show (a) TROPOMI NO$_2$ during the warm season (May–Sept 2019), (b) during the cold season (January–March and October–December 2019), and (c) the monthly variation in seven U.S. cities normalized to January 2019. Middle panels show (d) TROPOMI NO$_2$ when winds are <2 m/s, (e) when winds are >8 m/s, and (f) variations in NO$_2$ as a function of wind speed for seven cities normalized to stagnant conditions. Bottom panels show (g) TROPOMI NO$_2$ when winds are northeasterly, (h) when winds are southwesterly, and (i) variations as a function of wind direction for seven cities normalized to southwesterly winds. Wind variations are using the complete TROPOMI record preceding 1 January 2020 (1 May 2018 to 31 December 2019).

3.2. Effects of COVID-19 Physical Distancing on NO$_2$

In order to quantify rapid changes in NO$_x$ due to COVID-19 physical distancing, we calculate NO$_2$ changes in North American cities using three different methods and a reference method. The results for all cities are shown in Table 1.

The reference method, Method 0, compares the prelockdown and postlockdown periods and represents the "true" NO$_2$ change; however, this method does not account for seasonal changes and, thus, is not considered in the medians/means.

In Method 1, we compare an average of 15 March to 30 April 2020 to the same timeframe of 2019. In Figure 2, we show difference and ratio plots between these 2 years (i.e., Method 1). The largest decreases in NO$_2$ are near the major cities in North America. We also find regional decreases in the eastern North America. Conversely, the central and northwestern United States have seen little change between years, which is likely due to the high fraction of NO$_2$ attributed to biogenic sources and long-range transport. We also observe substantial decreases near retired electricity generating units in the western United States (Storrow, 2019).

In Figure 3, we demonstrate Method 2. Here, we show the 2019 and 2020 28-day running TROPOMI NO$_2$ medians after accounting for solar zenith angle, day-of-week patterns, and two meteorological factors: wind speed and wind direction. A 28-day period is chosen so as to best average out any random fluctuations not

Table 1
*Percentage Drop in Column NO$_2$ as Observed by TROPOMI*

City name	Reference case Method 0 Δ between months 2020 only (January–February vs. 15 March to 30 April)	Account for solar zenith angle only Method 1 Δ between years 2019 vs. 2020 (15 March to 30 April)	Account for solar zenith angle and meteorology Method 2 Using ERA5 analogs to account for meteorology 2019 versus 2020 (15 March to 30 April)	Method 3 Using GEM-MACH to infer NO$_2$, 2020 only (15 March to 30 April)	Mean of methods 1–3	Median of methods 1–3
San Jose	65.2%	43.4%	40.7%	43.5%	42.5%	**43.4%**
Los Angeles	66.1%	32.6%	32.5%	38.6%	34.6%	**32.6%**
Toronto	60.4%	31.0%	17.0%	42.0%	30.0%	**31.0%**
Philadelphia	50.3%	36.6%	30.7%	22.1%	29.8%	**30.7%**
Denver	25.8%	29.2%	23.4%	39.1%	30.6%	**29.2%**
Atlanta	39.6%	35.2%	27.4%	20.2%	27.6%	**27.4%**
Detroit	35.5%	29.9%	22.8%	15.6%	22.8%	**22.8%**
Boston	40.3%	22.8%	23.5%	17.8%	21.4%	**22.8%**
Washington DC	42.9%	31.4%	21.2%	6.7%	19.8%	**21.2%**
Montreal	12.5%	3.3%	20.9%	30.2%	18.1%	**20.9%**
New York City	32.7%	20.2%	20.0%	17.9%	19.4%	**20.0%**
New Orleans	41.7%	13.5%	19.6%	22.5%	18.5%	**19.6%**
Las Vegas	66.7%	9.5%	18.4%	42.0%	23.3%	**18.4%**
Houston	38.9%	26.3%	15.6%	1.9%	14.6%	**15.6%**
Chicago	31.0%	23.6%	14.9%	3.5%	14.0%	**14.9%**
Phoenix	43.9%	12.8%	14.8%	35.4%	21.0%	**14.8%**
Austin	34.3%	14.5%	9.4%	16.1%	13.3%	**14.5%**
Dallas	41.9%	11.9%	3.6%	16.7%	10.7%	**11.9%**
Miami	27.9%	16.1%	−1.6%	11.0%	8.5%	**11.0%**
Minneapolis	0.1%	14.3%	9.2%	8.1%	10.5%	**9.2%**
Mean of each method	39.9%	22.9%	19.2%	22.5%	21.6%	**21.6%**

associated with meteorological influences, such as missing data or real changes in NO$_x$ emissions due to temperature changes, but there may have been some fluctuations that cannot be averaged out. In Figure 3, the January values are uniformly lower than their true values (Figure S5) because we are normalizing to April meteorological conditions (i.e., solar zenith angle is lower in April as compared to January). In New York City, we calculate a 20.0% drop in NO$_2$ due to COVID-19 precautions. We find that there is no difference between Method 2—which accounts for meteorology—and Method 1—which only accounts for solar zenith angle. This suggests that varying meteorological conditions in New York City, while different between years, may not have had a strong biasing effect. However, in Washington D. C., we find favorable conditions in 2020 as compared to 2019 because we observe substantially different
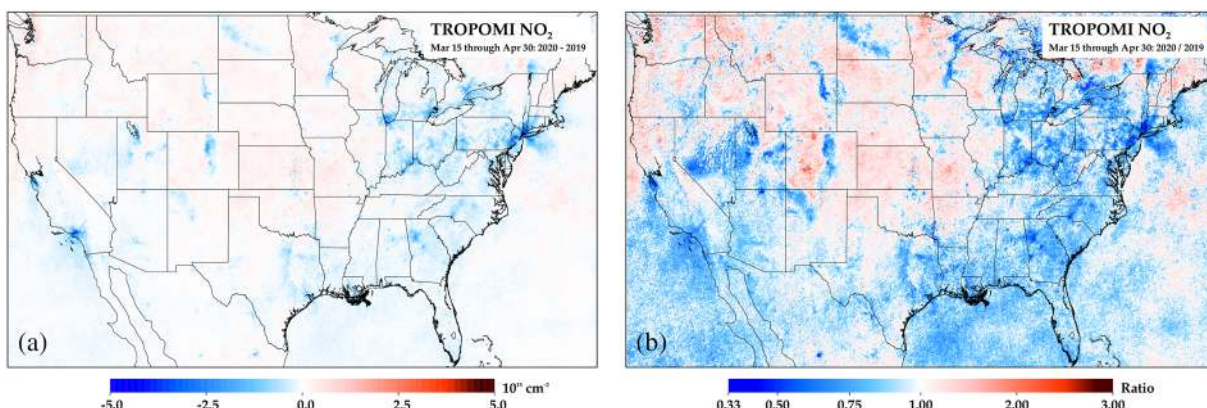
Figure 2. TROPOMI NO$_2$ differences between 2019 and 2020, using 15 March to 30 April 2020 as the post-COVID-19 period. Plots are showing (a) the absolute difference and (b) the ratio between years.
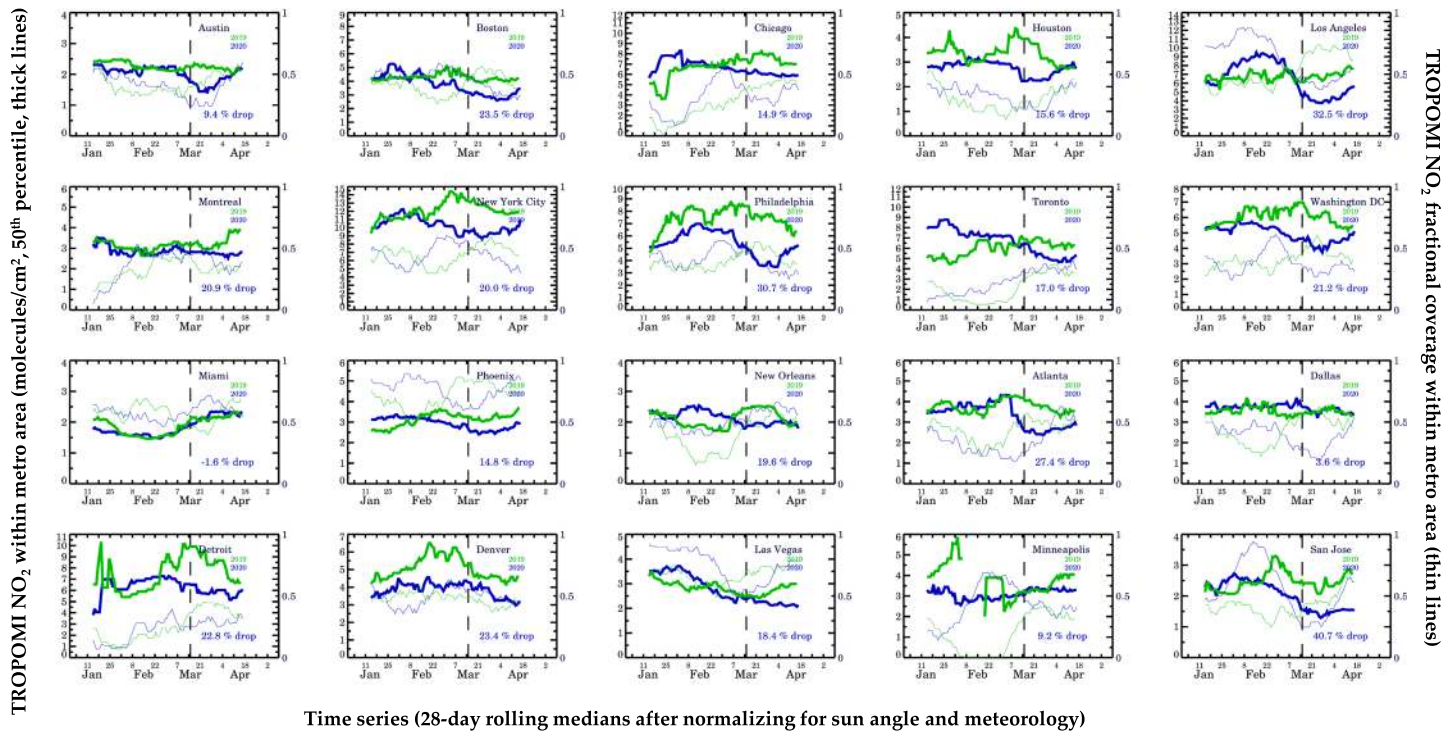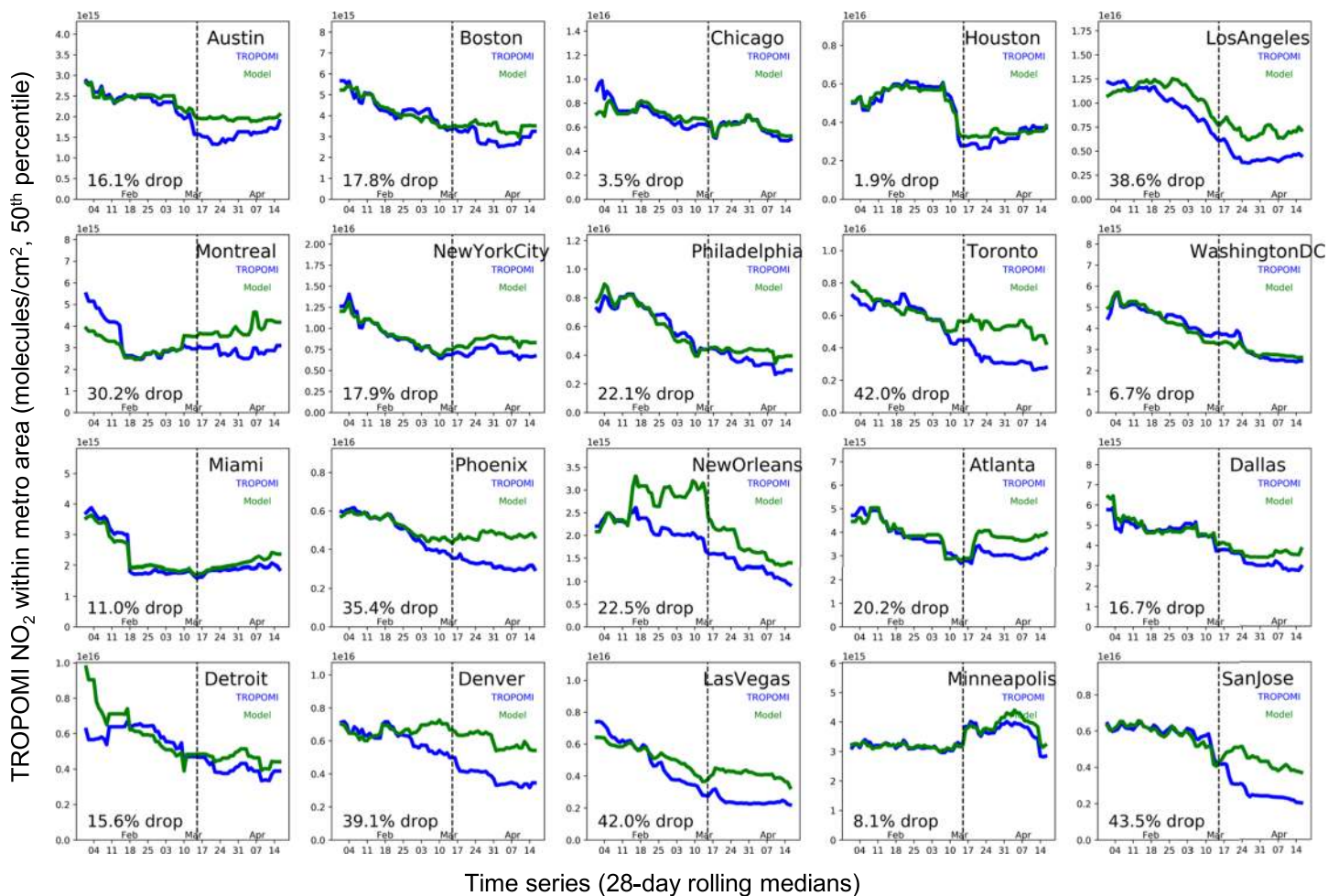
Figure 3. Trends in TROPOMI NO$_2$ since 1 January in 2019 and 2020 after accounting for meteorological variability and solar zenith angle. The thick lines represent the 28-day rolling median value (50th percentile) in a 0.4° × 0.4° box centered on the city center for the largest cities (New York City, Los Angeles, Chicago, Toronto, and Houston) and 0.2° × 0.2° box in all other cities. The thin lines represent the fractional coverage (0–1) in the coincident spatiotemporal domain.

NO$_2$ drops before (31.4%) and after (21.2%) correcting for the meteorology. These results are corroborated by the wind speed and direction (Figure S6). In 2019, winds were on average southwesterly, while in 2020, winds had more of a northwesterly and therefore cleaner component. Of all cities analyzed, we find that Miami had the most favorable conditions for low NO$_2$ in 2020 as compared to 2019; in 2020, winds were stronger from the south—in this case a cleaner air mass—than in 2019, which had relatively stagnant winds. Conversely, in Montreal, New Orleans, and Las Vegas, meteorological conditions appeared to be unfavorable in 2020 as compared to 2019.

Meteorological factors that we do not account for in Method 2 are a difference in the number of cloudy scenes and the amount of snow cover between years. In particular, the northern United States had more snow cover in late February and early March in 2019 than in 2020 (Figure S7). In Figure 3, we also show the fractional coverage of the metropolitan area during the 28-day period. For example, in New York City, there was ~0.6 fractional coverage in early March 2020, while in 2019 there was only ~0.3 fractional coverage during the same timeframe. As a result, some of the higher values during this timeframe may be related to fewer valid pixels in outlying areas, which retain snow for longer, and perhaps a snow-related reflectivity artifact even though pixels over snow cover are predominantly removed. This is also why some other snow-prone cities like Chicago, Philadelphia, Toronto, Detroit, Denver, and Minneapolis show large variability preceding March. Beginning in mid-March, snow cover was largely gone in most U.S. cities during both years.

In Figure 4, we demonstrate Method 3, in which we account for meteorology and chemical interactions using a chemical transport model. We create a theoretical TROPOMI column NO$_2$ using ECCC's regional operational air quality forecast model (Moran et al., 2009; Pendlebury et al., 2018), which accounts for typical seasonal emission changes but not for any impacts due to the COVID-19 lockdowns; this helps provide expected NO$_2$ levels with a business as usual scenario. Around mid-March there is often a divergence between the expected and observed NO$_2$ in the major cities. Using this method, largest NO$_2$ reductions

Figure 4. Trends in TROPOMI NO$_2$ since 1 January 2020. The actual observed columns are shown in black, while the "expected" columns—using GEM-MACH to infer NO$_2$ in the absence of lockdowns—is shown in blue. The lines represent the 28-day rolling median value (50th percentile) in a 0.4° × 0.4° box centered on the city center for the largest cities (New York City, Los Angeles, Chicago, Toronto, and Houston) and 0.2° × 0.2° box in all other cities.

due to COVID-19 precautions are in Toronto, San Jose, and Las Vegas. Similar to Method 2, we find that NO$_2$ changes are generally smaller in the Northeastern United States and Florida as compared to Method 1 after accounting for meteorology. In 15 of the 20 studied cities, we find that Methods 2 and 3, which utilize independent meteorological data sets, show similar biasing effects of meteorology (favorable vs. unfavorable) when compared to Method 1.

4. Conclusions and Discussion

We estimate that NO$_2$ adjusted for seasonality and meteorology temporarily dropped between 9–43% in North American cities due to COVID-19 precautions, with a median drop of 21.6% before and after COVID-19 physical distancing. If the solar zenith angle is not accounted for, then the median NO$_2$ drop is 39.9%; this represents the true change of NO$_2$ in cities, but is not particularly helpful if parsing out emissions changes. Our reported median drop of 21.6% after accounting for meteorology is marginally lower than the 22.9% in a simple year-to-year comparison, which suggests that 2020 meteorology was slightly favorable for lower NO$_2$, although these effects are most pronounced in the Northeastern United States and Florida.

Here we demonstrate two methodologies, Methods 2 and 3, to account for time-varying effects of meteorology on NO$_2$ concentrations. Although the NO$_2$ concentration is also function of collocated chemical constituents, such as OH, VOCs, and O$_3$, which also vary by year, the numbers reported here are closer to the true

change in NO_x emissions than NO_2 changes in the absence of accounting for meteorology. There are two main advantages for using Methods 2 and 3 to assess rapid changes in NO_x as compared to a year-to-year comparison of the same month or seasonal period. Year-over-year technological improvements in the North America are generally causing NO_x emissions to decrease over time (Goldberg, Lu, Oda, et al., 2019; Nopmongcol et al., 2017; Silvern et al., 2019; Zhang et al., 2018), although we find a statistically insignificant NO_2 increase of 0.6% in our cities between 2019 and 2020 in the January–February average. Accounting for year-over-year changes would be more important if comparing 2020 values to years preceding 2019. There are two U.S. cities, Denver and Philadelphia, which have consistently lower values in 2020 than in 2019 preceding March, using Method 2. While it is conceivable that there may have been policies in these two cities that yielded significantly lower NO_x emissions in 2020 versus 2019 preceding March, Method 3 does not corroborate this and further, we do not think the evidence is strong enough to conclude this given the uncertainty related to meteorological conditions unaccounted for, such as snow cover differences between years.

A deficiency of our method is our reliance on a single satellite instrument and algorithm. It is known that the operational TROPOMI NO_2 algorithm underestimates tropospheric vertical column NO_2 in urban areas due to its reliance on a global model to provide shape profiles for the air mass factor (AMF); investigating the effects of the AMF bias on trends will be the subject of future work. Also, there may be a clear-sky bias (Geddes et al., 2012) associated with TROPOMI retrievals, but the results presented here are generally consistent with studies using ground monitors over the coincident region (Bekbulat et al., 2020) and the reported CO_2 emissions reductions due to COVID-19 precautions (Le Quéré et al., 2020).

The estimates of NO_2 changes using our methods appear to be reasonable given a quick bottom-up emissions calculation. Initial statistics indicate vehicle miles traveled dropped by ~40% in April 2020 and that many industrial sources dropped modestly ~5–25% due to lockdown exemptions, NO_x reductions between 10% and 35% would be expected. San Jose, Los Angeles, and Toronto appear to have reductions at the high end of this range, while Miami, Minneapolis, and Dallas have values near the lowest end; further work will look into why these cities have reductions on the ends of the spectrum. Rapid assessments of NO_2 changes—after normalized for seasonal and meteorological factors—can be used to highlight locations that may have had greater changes in activity and better understand the sources contributing to adverse air quality in each city.

Data Availability Statement

TROPOMI NO_2 data can be freely downloaded from the European Space Agency Copernicus Open Access Hub or the NASA EarthData Portal (http://doi.org/10.5270/S5P-s4ljg54). The 100-m wind and 2-m surface temperatures from the ERA5 reanalysis can be freely downloaded from the Copernicus Climate Change (C3S) climate data store (CDS) (http://doi.org/10.24381/cds.adbb2d47) The intermediary data used to generate all figures can be found at http://doi.org/10.6084/m9.figshare.12721724. The submitted manuscript has been created by UChicago Argonne, LLC, Operator of Argonne National Laboratory ("Argonne"). Argonne, a U.S. Department of Energy Office of Science laboratory, is operated under Contract DE-AC02-06CH11357.

References

Abel, D. W., Holloway, T., Kladar, R. M., Meier, P., Ahl, D., Harkey, M., & Patz, J. (2017). Response of power plant emissions to ambient temperature in the eastern United States. *Environmental Science and Technology*, *51*(10), 5838–5846. https://doi.org/10.1021/acs.est.6b06201

Beirle, S., Boersma, K. F., Platt, U., Lawrence, M. G., & Wagner, T. (2011). Megacity emissions and lifetimes of nitrogen oxides probed from space. *Science*, *333*(6050), 1737–1739. https://doi.org/10.1126/science.1207824

Beirle, S., Borger, C., Dörner, S., Li, A., Hu, Z., Liu, F., et al. (2019). Pinpointing nitrogen oxide emissions from space. *Science Advances*, *5*(11), eaax9800. https://doi.org/10.1126/sciadv.aax9800

Beirle, S., Platt, U., Wenig, M., & Wagner, T. (2003). Weekly cycle of NO_2 by GOME measurements: A signature of anthropogenic sources. *Atmospheric Chemistry and Physics*, *3*(6), 2225–2232. https://doi.org/10.5194/acp-3-2225-2003

Bekbulat, B., Apte, J. S., Millet, D. B., Robinson, A. L., Wells, K., & Marshall, J. D. (2020). PM2.5 and ozone air pollution levels have not dropped consistently across the US following societal Covid response. Pre-print. https://doi.org/10.26434/CHEMRXIV.12275603

Boersma, K. F., Eskes, H. J., Richter, A., de Smedt, I., Lorente, A., Beirle, S., et al. (2018). Improving algorithms and uncertainty estimates for satellite NO2 retrievals: Results from the quality assurance for the essential climate variables (QA4ECV) project. *Atmospheric Measurement Techniques*, *11*(12), 6651–6678. https://doi.org/10.5194/amt-11-6651-2018

Copernicus Climate Change Service (C3S) (2017): ERA5: Fifth generation of ECMWF atmospheric reanalyses of the global climate. Copernicus Climate Change Service Climate Data Store (CDS), date of access. https://cds.climate.copernicus.eu/cdsapp#!/home

de Foy, B., Wilkins, J. L., Lu, Z., Streets, D. G., & Duncan, B. N. (2014). Model evaluation of methods for estimating surface emissions and chemical lifetimes from satellite data. *Atmospheric Environment*, *98*, 66–77. https://doi.org/10.1016/j.atmosenv.2014.08.051

Dix, B., Bruin, J., Roosenbrand, E., Vlemmix, T., Francoeur, C., Gorchov-Negron, A., et al. (2020). Nitrogen oxide emissions from U.S. oil and gas production: Recent trends and source attribution. *Geophysical Research Letters*, *47*, e2019GL085866. https://doi.org/10.1029/2019GL085866

Duncan, B. N., Lamsal, L. N., Thompson, A. M., Yoshida, Y., Lu, Z., Streets, D. G., et al. (2016). A space-based, high-resolution view of notable changes in urban NO$_x$ pollution around the world (2005–2014). *Journal of Geophysical Research: Atmospheres*, *121*, 976–996. https://doi.org/10.1002/2015JD024121

ESA (2020a). Air pollution drops in India following lockdown. Retrieved May 4, 2020, from http://www.esa.int/Applications/Observing_the_Earth/Copernicus/Sentinel-5P/Air_pollution_drops_in_India_following_lockdown

ESA (2020b). Coronavirus: Nitrogen dioxide emissions drop over Italy. Retrieved May 4, 2020, from http://www.esa.int/ESA_Multimedia/Videos/2020/03/Coronavirus_nitrogen_dioxide_emissions_drop_over_Italy

Geddes, J. A., Martin, R. V., Boys, B. L., & van Donkelaar, A. (2016). Long-term trends worldwide in ambient NO$_2$ concentrations inferred from satellite observations. *Environmental Health Perspectives*, *124*(3), 281–289. https://doi.org/10.1289/ehp.1409567

Geddes, J. A., Murphy, J. G., O'Brien, J. M., & Celarier, E. A. (2012). Biases in long-term NO$_2$ averages inferred from satellite observations due to cloud selection criteria. *Remote Sensing of Environment*, *124*(2), 210–216. https://doi.org/10.1016/j.rse.2012.05.008

Georgoulias, A. K., van Der, A. R. J., Stammes, P., Boersma, K. F., & Eskes, H. J. (2019). Trends and trend reversal detection in 2 decades of tropospheric NO$_2$ satellite observations. *Atmospheric Chemistry and Physics*, *19*(9), 6269–6294. https://doi.org/10.5194/acp-19-6269-2019

Goldberg, D. L., Lu, Z., Oda, T., Lamsal, L. N., Liu, F., Griffin, D., et al. (2019). Exploiting OMI NO$_2$ satellite observations to infer fossil-fuel CO$_2$ emissions from U.S. megacities. *Science of The Total Environment*, *695*, 133805. https://doi.org/10.1016/j.scitotenv.2019.133805

Goldberg, D. L., Lu, Z., Streets, D. G., de Foy, B., Griffin, D., McLinden, C. A., et al. (2019). Enhanced capabilities of TROPOMI NO$_2$: Estimating NO$_x$ from North American cities and power plants. *Environmental Science & Technology*, *53*(21), 12,594–12,601. https://doi.org/10.1021/acs.est.9b04488

Griffin, D., Zhao, X., McLinden, C. A., Boersma, F., Bourassa, A., Dammers, E., et al. (2019). High-resolution mapping of nitrogen dioxide with TROPOMI: First results and validation over the Canadian Oil Sands. *Geophysical Research Letters*, *46*, 1049–1060. https://doi.org/10.1029/2018GL081095

He, H., Hembeck, L., Hosley, K. M., Canty, T. P., Salawitch, R. J., & Dickerson, R. R. (2013). High ozone concentrations on hot days: The role of electric power demand and NO$_x$ emissions. *Geophysical Research Letters*, *40*, 5291–5294. https://doi.org/10.1002/grl.50967

Hilboll, A., Richter, A., & Burrows, J. P. (2013). Long-term changes of tropospheric NO$_2$ over megacities derived from multiple satellite instruments. *Atmospheric Chemistry and Physics*, *13*(8), 4145–4169. https://doi.org/10.5194/acp-13-4145-2013

Hilboll, A., Richter, A., & Burrows, J. P. (2017). NO$_2$ pollution over India observed from space—The impact of rapid economic growth, and a recent decline. *Atmospheric Chemistry and Physics Discussions*, *20*(2), 1–18. https://doi.org/10.5194/acp-2017-101

Holcombe, M., & O'Key, S. (2020). Satellite images show less pollution over the US as coronavirus shuts down public places. Retrieved from https://www.cnn.com/2020/03/23/health/us-pollution-satellite-coronavirus-scn-trnd/index.html

Ialongo, I., Virta, H., Eskes, H., Hovila, J., & Douros, J. (2020). Comparison of TROPOMI/Sentinel-5 precursor NO$_2$ observations with ground-based measurements in Helsinki. *Atmospheric Measurement Techniques*, *13*(1), 205–218. https://doi.org/10.5194/amt-13-205-2020

Kim, S.-W. W., Heckel, A., Frost, G. J., Richter, A., Gleason, J., Burrows, J. P., et al. (2009). NO$_2$ columns in the western United States observed from space and simulated by a regional chemistry model and their implications for NO$_x$ emissions. *Journal of Geophysical Research*, *114*, D11301. https://doi.org/10.1029/2008JD011343

Krotkov, N. A., McLinden, C. A., Li, C., Lamsal, L. N., Celarier, E. A., Marchenko, S. V., et al. (2016). Aura OMI observations of regional SO$_2$ and NO$_2$ pollution changes from 2005 to 2015. *Atmospheric Chemistry and Physics*, *16*(7), 4605–4629. https://doi.org/10.5194/acp-16-4605-2016

Lamsal, L. N., Duncan, B. N., Yoshida, Y., Krotkov, N. A., Pickering, K. E., Streets, D. G., & Lu, Z. (2015). U.S. NO$_2$ trends (2005–2013): EPA Air Quality System (AQS) data versus improved observations from the Ozone Monitoring Instrument (OMI). *Atmospheric Environment*, *110*(2), 130–143. https://doi.org/10.1016/j.atmosenv.2015.03.055

Laughner, J. L., & Cohen, R. C. (2019). Direct observation of changing NO$_x$ lifetime in North American cities. *Science*, *366*(6466), 723–727. https://doi.org/10.1126/science.aax6832

Le Quéré, C., Jackson, R. B., Jones, M. W., Smith, A. J., Abernethy, S., Andrew, R. M., et al. (2020). Temporary reduction in daily global CO$_2$ emissions during the COVID-19 forced confinement. *Nature Climate Change*, *10*, 647–653. https://doi.org/10.1038/s41558-020-0797-x

Liu, F., Page, A., Strode, S. A., Yoshida, Y., Choi, S., Zheng, B., et al. (2020). Abrupt declines in tropospheric nitrogen dioxide over China after the outbreak of COVID-19. *Science Advances*, *6*(28), eabc2992. https://doi.org/10.1126/sciadv.abc2992

McLinden, C. A., Fioletov, V. E., Krotkov, N. A., Li, C., Boersma, K. F., & Adams, C. (2016). A decade of change in NO$_2$ and SO$_2$ over the Canadian Oil Sands as seen from space. *Environmental Science and Technology*, *50*(1), 331–337. https://doi.org/10.1021/acs.est.5b04985

Moran, M. D., Ménard, S., Talbot, D., Huang, P., Makar, P. A., Gong, W., et al. (2009). Particulate-matter forecasting with GEM-MACH15, A New Canadian Air-Quality Forecast Model. In Air Pollution Modeling and Its Application XX. Retrieved from http://www.nato.int/science

NASA (2020). Pandemic before and after: Northeast US 2015–2019 versus 2020. Retrieved from https://airquality.gsfc.nasa.gov/slider/northeast-2020

Nopmongcol, U., Alvarez, Y., Jung, J., Grant, J., Kumar, N., & Yarwood, G. (2017). Source contributions to United States ozone and particulate matter over five decades from 1970 to 2020. *Atmospheric Environment*, *167*(2017), 116–128. https://doi.org/10.1016/j.atmosenv.2017.08.009

Pendlebury, D., Gravel, S., Moran, M. D., & Lupu, A. (2018). Impact of chemical lateral boundary conditions in a regional air quality forecast model on surface ozone predictions during stratospheric intrusions. *Atmospheric Environment*, *174*, 148–170. https://doi.org/10.1016/j.atmosenv.2017.10.052

Plumer, B., & Popovich, N. (2020). Traffic and pollution plummet as U.S. cities shut down for coronavirus. Retrieved from https://www.nytimes.com/interactive/2020/03/22/climate/coronavirus-usa-traffic.html

Pope, R. J., Chipperfield, M. P., Savage, N. H., Ordóñez, C., Neal, L. S., Lee, L. A., et al. (2015). Evaluation of a regional air quality model using satellite column NO$_2$: Treatment of observation errors and model boundary conditions and emissions. *Atmospheric Chemistry and Physics*, *15*(10), 5611–5626. https://doi.org/10.5194/acp-15-5611-2015

Geophysical Research Letters

Reuter, M., Buchwitz, M., Schneising, O., Krautwurst, S., O'Dell, C. W., Richter, A., et al. (2019). Towards monitoring localized CO_2 emissions from space: Co-located regional CO_2 and NO_2 enhancements observed by the OCO-2 and S5P satellites. *Atmospheric Chemistry and Physics*, *19*(14), 9371–9383. https://doi.org/10.5194/acp-19-9371-2019

Shah, V., Jacob, D. J., Li, K., Silvern, R. F., Zhai, S., Liu, M., et al. (2020). Effect of changing NO_x lifetime on the seasonality and long-term trends of satellite-observed tropospheric NO_2 columns over China. *Atmospheric Chemistry and Physics*, *20*(3), 1483–1495. https://doi.org/10.5194/acp-20-1483-2020

Silvern, R. F., Jacob, D. J., Mickley, L. J., Sulprizio, M. P., Travis, K. R., Marais, E. A., et al. (2019). Using satellite observations of tropospheric NO_2 columns to infer long-term trends in US NO_x emissions: The importance of accounting for the free tropospheric NO_2 background. *Atmospheric Chemistry and Physics*, *19*(13), 8863–8878. https://doi.org/10.5194/acp-19-8863-2019

Stavrakou, T., Müller, J.-F., Boersma, K. F., van Der, A. R. J., Kurokawa, J., Ohara, T., & Zhang, Q. (2013). Key chemical NO_x sink uncertainties and how they influence top-down emissions of nitrogen oxides. *Atmospheric Chemistry and Physics*, *13*(17), 9057–9082. https://doi.org/10.5194/acp-13-9057-2013

Storrow, B. (2019). America's mega-emitters are starting to close. Retrieved May 15, 2020, from https://www.eenews.net/stories/1060965553/

Valin, L. C., Russell, A. R., & Cohen, R. C. (2013). Variations of OH radical in an urban plume inferred from NO_2 column measurements. *Geophysical Research Letters*, *40*, 1856–1860. https://doi.org/10.1002/grl.50267

van Der, A. R. J., Eskes, H. J., Boersma, K. F., Van Noije, T. P. C., Van Roozendael, M., De Smedt, I., et al. (2008). Trends, seasonal variability and dominant NO_x source derived from a ten year record of NO_2 measured from space. *Journal of Geophysical Research*, *113*(D4), 1, D04302–12. https://doi.org/10.1029/2007JD009021

van Geffen, J. H. G. M., Eskes, H. J., Boersma, K. F., Maasakkers, J. D., & Veefkind, J. P. (2019). TROPOMI ATBD of the total and tropospheric NO_2 data products. Retrieved from http://www.tropomi.eu/sites/default/files/files/publicS5P-KNMI-L2-0005-RP-ATBD_NO2_data_products-20190206_v140.pdf

Veefkind, J. P., Aben, I., McMullan, K., Förster, H., de Vries, J., Otter, G., et al. (2012). TROPOMI on the ESA Sentinel-5 precursor: A GMES mission for global observations of the atmospheric composition for climate, air quality and ozone layer applications. *Remote Sensing of Environment*, *120*(2012), 70–83. https://doi.org/10.1016/j.rse.2011.09.027

Wang, C., Wang, T., & Wang, P. (2019). The spatial–temporal variation of tropospheric NO_2 over China during 2005 to 2018. *Atmosphere*, *10*(8), 444. https://doi.org/10.3390/atmos10080444

Zhang, R., Wang, Y., Smeltzer, C., Qu, H., Koshak, W., & Folkert Boersma, K. (2018). Comparing OMI-based and EPA AQS in situ NO_2 trends: Towards understanding surface NO_x emission changes. *Atmospheric Measurement Techniques*, *11*(7), 3955–3967. https://doi.org/10.5194/amt-11-3955-2018

Zhang, R., Zhang, Y., Lin, H., Feng, X., Fu, T.-M., & Wang, Y. (2020). NO_x emission reduction and recovery during COVID-19 in East China. *Atmosphere*, *11*(4), 433. https://doi.org/10.3390/atmos11040433

Zhao, X., Griffin, D., Fioletov, V., McLinden, C., Cede, A., Tiefengraber, M., et al. (2020). Assessment of the quality of TROPOMI high-spatial-resolution NO_2 data products in the Greater Toronto Area. *Atmospheric Measurement Techniques*, *13*(4), 2131–2159. https://doi.org/10.5194/amt-13-2131-2020

References From the Supporting Information

Bey, I., Jacob, D. J., Yantosca, R. M., Logan, J. A., Field, B. D., Fiore, A. M., et al. (2001). Global modeling of tropospheric chemistry with assimilated meteorology: Model description and evaluation. *Journal of Geophysical Research*, *106*(D19), 23,073–23,095. https://doi.org/10.1029/2001JD000807

Choi, S., Lamsal, L. N., Follette-Cook, M., Joiner, J., Krotkov, N. A., Swartz, W. H., et al. (2019). Assessment of NO_2 observations during DISCOVER-AQ and KORUS-AQ field campaigns. *Atmospheric Measurement Techniques*, *13*(5), 2523–2546. https://doi.org/10.5194/amt-13-2523-2020

Coats, C. J. (1996). High-performance algorithms in the Sparse Matrix Operator Kernel Emissions (SMOKE) Modeling System, American Meteorological Society, Atlanta, GA. USA, Proceedings of the Ninth AMS Joint Conference on Applications of Air Pollution Meteorology with AWMA.

Côté, J., Gravel, S., Méthot, A., Patoine, A., Roch, M., & Staniforth, A. (1998). The operational CMC–MRB Global Environmental Multiscale (GEM) model. Part I: Design considerations and formulation. *Monthly Weather Review*, *126*(6), 1373–1395. https://doi.org/10.1175/1520-0493(1998)126<1373:TOCMGE>2.0.CO;2

Goldberg, D. L., Anenberg, S. C., Mohegh, A., Lu, Z., & Streets, D. G. (2020). TROPOMI NO_2 in the United States: A detailed look at the annual averages, weekly cycles, effects of temperature, and correlation with PM2.5. https://doi.org/10.1002/essoar.10503422.1

Goldberg, D. L., Lamsal, L. N., Loughner, C. P., Swartz, W. H., Lu, Z., & Streets, D. G. (2017). A high-resolution and observationally constrained OMI NO_2 satellite retrieval. *Atmospheric Chemistry and Physics*, *17*(18), 11,403–11,421. https://doi.org/10.5194/acp-17-11403-2017

Ialongo, I., Herman, J. R., Krotkov, N., Lamsal, L. N., Folkert Boersma, K., Hovila, J., & Tamminen, J. (2016). Comparison of OMI NO_2 observations and their seasonal and weekly cycles with ground-based measurements in Helsinki. *Atmospheric Measurement Techniques*, *9*(10), 5203–5212. https://doi.org/10.5194/amt-9-5203-2016

Kleipool, Q. L., Dobber, M. R., de Haan, J. F., & Levelt, P. F. (2008). Earth surface reflectance climatology from 3 years of OMI data. *Journal of Geophysical Research*, *113*, D18308. https://doi.org/10.1029/2008JD010290

Lamsal, L. N., Krotkov, N. A., Celarier, E. A., Swartz, W. H., Pickering, K. E., Bucsela, E. J., et al. (2014). Evaluation of OMI operational standard NO_2 column retrievals using in situ and surface-based NO_2 observations. *Atmospheric Chemistry and Physics*, *14*(21), 11,587–11,609. https://doi.org/10.5194/acp-14-11587-2014

Laughner, J. L., Zare, A., & Cohen, R. C. (2016). Effects of daily meteorology on the interpretation of space-based remote sensing of NO_2. *Atmospheric Chemistry and Physics*, *16*(23), 15,247–15,264. https://doi.org/10.5194/acp-16-15247-2016

Laughner, J. L., Zhu, Q., & Cohen, R. C. (2019). Evaluation of version 3.0B of the BEHR OMI NO_2 product. *Atmospheric Measurement Techniques*, *12*(1), 129–146. https://doi.org/10.5194/amt-12-129-2019

Lin, J. T., Liu, M. Y., Xin, J. Y., Boersma, K. F., Spurr, R., Martin, R. V., & Zhang, Q. (2015). Influence of aerosols and surface reflectance on satellite NO_2 retrieval: Seasonal and spatial characteristics and implications for NO_x emission constraints. *Atmospheric Chemistry and Physics*, *15*(19), 11,217–11,241. https://doi.org/10.5194/acp-15-11217-2015

Liu, M., Lin, J., Boersma, K. F., Pinardi, G., Wang, Y., Chimot, J., et al. (2019). Improved aerosol correction for OMI tropospheric NO$_2$ retrieval over East Asia: Constraint from CALIOP aerosol vertical profile. *Atmospheric Measurement Techniques*, *12*(1), 1–21. https://doi.org/10.5194/amt-12-1-2019

Lorente, A., Folkert Boersma, K., Yu, H., Dörner, S., Hilboll, A., Richter, A., et al. (2017). Structural uncertainty in air mass factor calculation for NO$_2$ and HCHO satellite retrievals. *Atmospheric Measurement Techniques*, *10*(3), 759–782. https://doi.org/10.5194/amt-10-759-2017

McLinden, C. A., Fioletov, V., Boersma, K. F., Kharol, S. K., Krotkov, N., Lamsal, L., et al. (2014). Improved satellite retrievals of NO$_2$ and SO$_2$ over the Canadian oil sands and comparisons with surface measurements. *Atmospheric Chemistry and Physics*, *14*(7), 3637–3656. https://doi.org/10.5194/acp-14-3637-2014

Palmer, P. I., Jacob, D. J., Chance, K., Martin, R. V., Spurr, R. J. D., Kurosu, T. P., et al. (2001). Air mass factor formulation for spectroscopic measurements from satellites: Application to formaldehyde retrievals from the Global Ozone Monitoring Experiment. *Journal of Geophysical Research*, *106*(D13), 14,539–14,550. https://doi.org/10.1029/2000JD900772

Russell, A. R., Perring, A. E., Valin, L. C., Bucsela, E. J., Browne, E. C., Wooldridge, P. J., & Cohen, R. C. (2011). A high spatial resolution retrieval of NO$_2$ column densities from OMI: Method and evaluation. *Atmospheric Chemistry and Physics*, *11*(16), 8543–8554. https://doi.org/10.5194/acp-11-8543-2011

Russell, A. R., Valin, L. C., Bucsela, E. J., Wenig, M. O., & Cohen, R. C. (2010). Space-based constraints on spatial and temporal patterns of NO$_x$ emissions in California, 2005–2008. *Environmental Science and Technology*, *44*(9), 3608–3615. https://doi.org/10.1021/es903451j

Stavrakou, T., Müller, J.-F., Bauwens, M., Boersma, K. F., & van Geffen, J. (2020). Satellite evidence for changes in the NO$_2$ weekly cycle over large cities. *Scientific Reports*, *10*(1), 10066. https://doi.org/10.1038/s41598-020-66891-0

van Geffen, J., Boersma, K. F., Eskes, H., Sneep, M., ter Linden, M., Zara, M., & Veefkind, J. P. (2020). S5P TROPOMI NO$_2$ slant column retrieval: Method, stability, uncertainties and comparisons with OMI. *Atmospheric Measurement Techniques*, *13*(3), 1315–1335. https://doi.org/10.5194/amt-13-1315-2020

Williams, J. E., Folkert Boersma, K., Le Sager, P., & Verstraeten, W. W. (2017). The high-resolution version of TM5-MP for optimized satellite retrievals: Description and validation. *Geoscientific Model Development*, *10*(2), 721–750. https://doi.org/10.5194/gmd-10-721-2017